nature chemical biology

ARTICLE

PUBLISHED ONLINE: 19 JANUARY 2014 | DOI: 10.1038/NCHEMBIO.1436

Allostery in Ca^{2+} channel modulation by calcium-binding proteins

Philemon S Yang[1], Manu Ben Johny[1] & David T Yue[1,2]*

Distinguishing between allostery and competition among modulating ligands is challenging for large target molecules. Out of practical necessity, inferences are often drawn from *in vitro* assays on target fragments, but such inferences may belie actual mechanisms. One key example of such ambiguity concerns calcium-binding proteins (CaBPs) that tune signaling molecules regulated by calmodulin (CaM). As CaBPs resemble CaM, CaBPs are believed to competitively replace CaM on targets. Yet, brain CaM expression far surpasses that of CaBPs, raising questions as to whether CaBPs can exert appreciable biological actions. Here, we devise a live-cell, holomolecule approach that reveals an allosteric mechanism for calcium channels whose CaM-mediated inactivation is eliminated by CaBP4. Our strategy is to covalently link CaM and/or CaBP to holochannels, enabling live-cell fluorescence resonance energy transfer assays to resolve a cyclical allosteric binding scheme for CaM and CaBP4 to channels, thus explaining how trace CaBPs prevail. This approach may apply generally for discerning allostery in live cells.

Distinct modulatory ligands frequently act upon common target molecules[1–3], supporting molecular computations important to biological signaling networks[3,4]. These ligands may act by competition, wherein only one ligand can bind at a time, or by allostery, allowing simultaneous interaction[5]. This contrast in classic biochemical mechanism holds crucial implications for signaling behavior but can be notoriously difficult to establish[6]. This is particularly true for large target molecules resistant to reconstitution outside of live cells. If studied piecemeal as subdomain peptides, such targets often exhibit multiple potential ligand-binding sites, but the relevance of these within the holomolecule often remains uncertain[7].

One prime example of such mechanistic ambiguity concerns the interaction of voltage-gated Ca^{2+} channels (Ca_V) with two modulatory ligands: CaM and CaBPs. To start, CaM regulation of Ca_V channels has a major role in the intracellular Ca^{2+} feedback orchestrating many biological processes[8]. This modulation frequently manifests as a Ca^{2+}-dependent inactivation (CDI) of channel opening[9,10], which is important for Ca^{2+} homeostasis[11]. Additionally, exciting recent discoveries identify CaBPs, a family of CaM-like brain molecules[12–17], that may also bind Ca_V channels and other targets[18,19]. CaBPs are bilobed like CaM, with each lobe containing two EF-hand Ca^{2+}-binding motifs[12]. However, though all four EF hands bind Ca^{2+} in CaM, one of them is nonfunctional in CaBPs. Coexpressing CaBPs with Ca_V1 channels then eliminates their CDI[14,20]. Indeed, modulation like this diversifies biological responses to Ca^{2+} signals[13,14,18,21].

Given the similarity of CaM and CaBPs, the prevailing hypothesis is that CaBPs competitively replace CaM on channels[14,22,23]. Indeed, these ligands exhibit competitive binding to an isolated channel IQ domain (**Fig. 1a**), a principal element for CDI. The interaction of CaM and CaBPs may thus be formulated as in **Figure 1b**. State 1 portrays an 'empty' channel without ligand that is thus incapable of CaM-mediated Ca^{2+} regulation[24,25]. This empty channel may bind CaM at the IQ domain to form a complex (state 2) that can then undergo Ca^{2+} regulation (for example, inactivation). Alternatively, CaBP may bind at the IQ domain, yielding a state 3 with altered Ca^{2+} regulatory behavior (for example, being noninactivatable). Importantly, both CaM and CaBP cannot simultaneously bind (state 4 excluded) under competition. Hypothetical dispositions of CaBP and CaM are shown in **Figure 1b**.

As with many large molecules, studies of isolated channel peptides raise the possibility of more complex scenarios. Specifically, peptide assays hint at multiple potential binding sites for CaM and CaBPs. Thus, these two ligands need not compete at the IQ domain, and the possibility of an allosteric mechanism arises (**Fig. 1b**). For CaM regulation itself, interaction sites extend beyond the IQ domain (**Fig. 1a**). In fact, CaM regulation starts with a single apoCaM (Ca^{2+}-free CaM) preassociated with the C-lobe of apoCaM embracing the IQ domain[24–27] (**Fig. 1a**) and with the N-lobe engaging upstream vestigial EF hands[24] (**Fig. 1a**), all within an encompassing Ca^{2+}-inactivating (CI) region[9,28,29]. Ca^{2+} binding to this 'resident' CaM alters channel opening by driving rearrangements that may include the binding of the N-lobe of Ca^{2+}-bound CaM (Ca^{2+}-CaM) to the channel amino terminus[30] (**Fig. 1a**). Regarding CaBPs, peptide assays also hint at interactions beyond the IQ domain[31,32], but the relevance of these assays to holochannels remains unsettled. One study argues for the functional impact of such sites[32], whereas another argues otherwise[31]. In all, the scheme of CaM and CaBP interaction remains ambiguous (**Fig. 1b**), and clear tests for concurrent ligand binding to holochannels (i.e., state 4) have proven infeasible. This state of impasse is common to many large molecules[33,34].

Importantly, the distinctions between competitive versus allosteric mechanism concern more than academic interest; they seem to be critical to the biological activity of CaBPs. In particular, the affinity of Ca_V channels for apoCaM may be greater than that for CaBPs[14,25,26], as the present study substantiates. Moreover, this study highlights a predominance of CaM over CaBP expression throughout the brain. Under competition, then, how could CaBPs exert functional effects? By contrast, an allosteric mechanism with the right mix of parameters would readily explain how naturally occurring CaBPs could still exert modulation.

Here, we establish an allosteric mechanism for $Ca_V1.3$ Ca^{2+} channels, a robust prototype system where strong CaM-mediated CDI can nonetheless be completely suppressed by CaBPs. Our approach is to exploit covalent linkage of holochannels to CaM and/or CaBP, along with live-cell fluorescence resonance energy

[1]Calcium Signals Laboratory, Department of Biomedical Engineering, The Johns Hopkins University School of Medicine, Baltimore, Maryland, USA. [2]Department of Neuroscience, The Johns Hopkins University School of Medicine, Baltimore, Maryland, USA. *e-mail: dyue@bme.jhu.edu

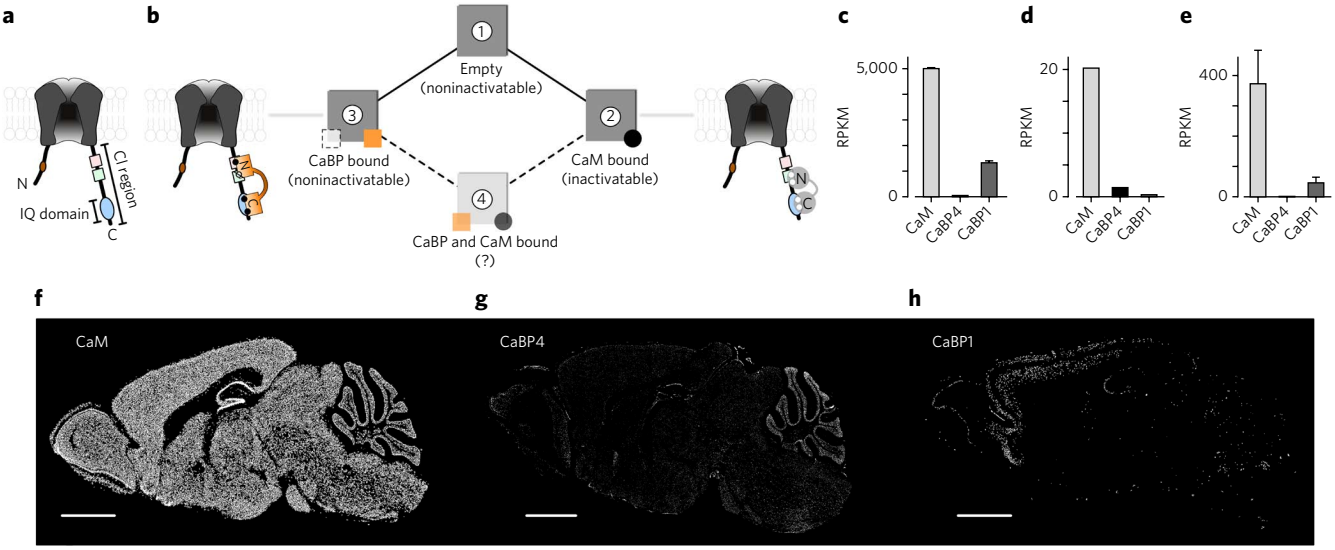

Figure 1 | Potential mechanisms of CaM and CaBP interaction with calcium channels. (**a**) Calcium channel landmarks. The CI region (~160 residues of proximal C terminus) contains elements involved in CaM regulation. The IQ domain (blue oval) harbors apoCaM preassociation and is the proposed site of CaBP interaction. Also shown are vestigial EF hands (squares), the NSCaTE element (brown oval) and the N-lobe Ca^{2+}-CaM effector site. (**b**) Potential mechanisms of CaM and CaBP interaction. The prevailing competitive hypothesis restricts model to states 1–3 and excludes state 4. In state 1, the channel lacks both CaM and CaBP. In state 2, the channel has a single apoCaM bound (black circle), primarily to the IQ domain. In state 3, the channel has a single CaBP bound (orange square). Under competition, CaBP would occupy the same site as CaM (i.e., IQ domain), allowing channel binding to either ligand but not both. Under allostery, CaBP binds the alternate site (state 3, dashed outline square), allowing simultaneous binding of CaM and CaBP (state 4). The existence of state 4 is unknown. At far right and left is the hypothetical interaction of CaBP (left) and CaM (right) with the IQ element under competition. (**c**) Relative transcript count (reads per kilobase million (RPKM)) of CaM, CaBP4 and CaBP1, obtained by deep sequencing of transcriptomes from the adult mouse neocortex. (**d**) Serial analysis of gene expression reveals transcript levels from adult mouse retina. CaM expression is ~15× that of CaBP4 and ~70× that of CaBP1. (**e**) Deep sequencing of transcriptomes from human prefrontal cortex. CaM transcripts are ~8× that of CaBP1 and ~6,000× that of CaBP4. (**f**–**h**) *In situ* hybridization mouse brain images using CaM (**f**), CaBP4 (**g**) and CaBP1 (**h**) from Allen Brain Atlas, normalized by scaling neocortical region to match RPKM signals in **c**. Scale bars, 2 mm.

transfer (FRET) binding assays with intact holochannel complexes. In so doing, we fully resolve a cyclical allosteric binding scheme for CaM and CaBP4 to channels (**Fig. 1b**). The parameters we obtain explain how trace CaBP can functionally prevail over excess CaM. This approach may furnish a general means for discriminating allosteric mechanisms in the live-cell context.

RESULTS

Predominance of CaM over CaBPs in the CNS

To motivate exploration of competitive versus allosteric mechanisms, we first considered the relative expression of CaM and CaBPs in the central nervous system (CNS). Given a competitive mechanism of CaBP modulation of Ca^{2+} channels, CaBP must at least approach the abundance of CaM to be functionally relevant, particularly if channels are to exhibit a greater affinity for apoCaM over CaBPs. In native systems, however, CaBP expression pales in comparison to that for CaM[35], even for the more prominent CaBP1 and CaBP4 isoforms. Deep sequencing in mouse neocortex[36] reveals CaBP1 transcripts to be ~5-fold more rare than those for CaM, and CaBP4 transcripts are 10,000-fold more rare (**Fig. 1c**). Similarly, serial analysis of gene expression analysis of whole mouse retina[37] estimates a 1:15 ratio for CaBP4 to CaM transcripts and an even smaller ratio for CaBP1 (**Fig. 1d**). Moreover, deep sequencing of human prefrontal cortex[38] indicates a 1:8 ratio for CaBP1 to CaM transcripts and a 1:6,000 ratio for CaBP4 (**Fig. 1e**). Although transcript abundance is not equivalent to protein expression, the enormous degree of transcript imbalance here would certainly yield protein expression mismatch[39]. Normalized *in situ* hybridization profiles of mouse brain (**Fig. 1f–h**) underscore the predominance of CaM[35], raising a challenge for competitive mechanisms and prompting a search for potential allostery.

As a critical prelude to this search, we sought to resolve the functional contribution of ancillary CaBP binding sites outside the IQ domain, especially within the relevant configuration of the holochannel complex. This step would be a necessary ante for considering an allosteric scenario. Thus, we undertook a two-step sequence: first, to consolidate the baseline functional effects and binding properties of CaBP to $Ca_V1.3$ channels, and second, to validate the functional relevance of potential ancillary CaBP binding sites in chimeric Ca^{2+} channels.

CaBP modulation and binding of $Ca_V1.3$ channels

Figure 2a displays the baseline effects of CaBPs on $Ca_V1.3$ channels. We mainly focused on the rarer CaBP4 isoform because it faces the larger competitive challenge. Absent CaBP, CaM-mediated CDI triggers strong decay of Ca^{2+} current[14] when compared to Ba^{2+}. Ba^{2+} binds CaM poorly[40] and thus furnishes a baseline reference without CDI. Upon strong overexpression of CaBP4, CDI is eliminated in exemplar traces[14]. Population data in **Figure 2b** fully confirm these trends, where the fraction of peak current remaining after 300-ms depolarization (r_{300}) gauges steady-state inactivation. When plotted versus step potential, the r_{300} relation obtained with Ba^{2+} is nearly flat, corroborating weak voltage-dependent inactivation. In control, the corresponding Ca^{2+} r_{300} relation exhibits a U shape, indicating genuine CDI[9]. The difference between these relations (f_{300}, at 10-mV step depolarization) then quantifies CDI in isolation. Upon coexpression of CaBP4, the Ba^{2+} and Ca^{2+} relations coalesce, substantiating elimination of CDI. **Figure 2c** portrays this effect in f_{300} bar graph format, used for compactness in subsequent figures.

Regarding binding, CaBP4 might outcompete excess CaM if CaBP4 were to exhibit a higher affinity for channels than CaM.

Prior peptide assays conflict on this point[14,27], and quantification of CaM and CaBP4 binding to functional holochannel complexes has seldom been achieved. We previously developed a holochannel FRET 2-hybrid assay[26,41] enabling characterization of CaM binding to functional $Ca_V1.2$ in live cells. Here, we use this approach to quantify interaction between YFP-tagged $Ca_V1.3$ channels and CFP-tagged CaM or CaBP4 (**Fig. 2d,e**). Within the scheme in **Figure 1b**, these assays measure the association constants between states 1 and 2 (**Fig. 2d**) and between states 1 and 3 (**Fig. 2e**). The rightmost subpanel in **Figure 2d** plots FRET efficiency (E_A) versus the relative free concentration of apoCaM (D_{free}), yielding a binding curve with a large association constant of K_{12} = 44 ± 9 μM^{-1} ($K_{a,EFF}$ = 143 × 10^{-5} microscope-specific units). By contrast, though CaBP4 does bind well to the channel (**Fig. 2e**), the affinity is ten-fold lower with a K_a = 4.4 ± 0.7 μM^{-1}. Likewise, CaBP1 binding was 2.6 ± 0.4 μM^{-1} (**Supplementary Results**, **Supplementary Fig. 1**). Of note, interaction affinity ($K_{a,EFF}$) is the reciprocal of the free concentration of donor-tagged molecules (D_{free}) at half-maximal E_A, whereas the distance and orientation of donor and acceptor fluorophores in the bound complex specifies maximal E_A ($E_{A/max}$) at large D_{free} values[26,41].

To identify candidate segments for CaBP4 binding with holochannels (**Fig. 2e**), we scanned the intracellular loops of $Ca_V1.3$ for CaBP4 interaction (**Fig. 2e**) using a peptide version of FRET 2-hybrid assays[26,41]. CaBP4–ECFP was the donor, and EYFP fused to various channel segments was the acceptor. Though peptide affinities may not translate quantitatively to the intact context, they serve to identify regions meriting full analysis via integrative holochannel assays. **Figure 2f** confirms CaBP4 binding to the isolated IQ domain of $Ca_V1.3$, as observed previously[14,27]. Notably, the interaction affinity is lower than that for the holochannel (gray fit), suggesting that other segments contribute. Indeed, CaBP4 also interacts with the upstream proximal Ca^{2+}-inactivating (PCI) region shown in **Figure 2g**, and further results identify other candidate interaction sites at the channel amino terminus and the C-terminal third of the loop between domains III and IV (III-IV loop) (**Fig. 2h** and **Supplementary Fig. 2**). These findings largely agree with those in homologous $Ca_V1.2$ channels[20,22].

Donating CaBP4 modulation to chimeric channels

To test for functional relevance of candidate CaBP4 binding segments (**Fig. 2h**) at the holochannel level, we sought to confer CaBP4 sensitivity to CaBP-insensitive channels via donation of essential $Ca_V1.3$ modules. We thus turned to the $Ca_V2.3$ isoform (**Fig. 3a** and

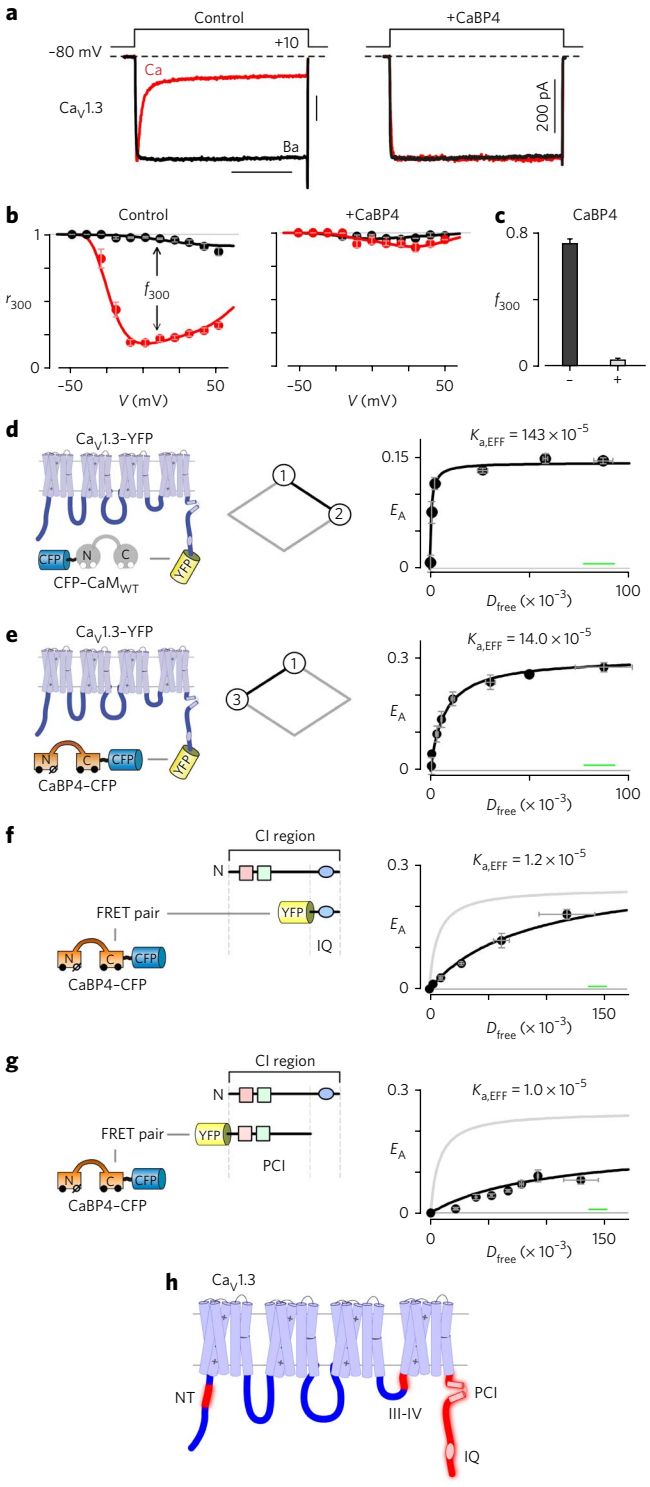

Figure 2 | CaBP4 modulation and binding of $Ca_V1.3$ channels. (**a**) Functional CaBP4 effects on whole-cell $Ca_V1.3$ current traces. Left, CaM-mediated CDI without CaBP4. Scale bar pertains to Ca^{2+} currents (red) and represents 100 ms. Ba^{2+} currents (black) were scaled down ~3× for comparison of decay kinetics (this format is used throughout all figures). Right, coexpressing CaBP4 eliminates CDI. (**b**) Population data confirming CaBP4 elimination of CDI. Left, fraction of peak current after 300-ms depolarization (r_{300}) versus step voltage for control cells. Black represents Ba^{2+} currents and red represents Ca^{2+} currents (mean ± s.e.m., n = 7 cells). Difference between relations at +10 mV (f_{300}) reports steady-state CDI[14]. Right, elimination of CDI by CaBP4 (n = 7). (**c**) Bar graph summary for relations in **b** (n = 7). (**d**) Left, cartoon of FRET 2-hybrid pairs: $Ca_V1.3$ fused with YFP on C terminus ($Ca_V1.3$–YFP) and CFP–CaM_{WT}. Middle, diamond schematic (**Fig. 1b**) showing predominant transition (black segment) as probed by FRET experiments. Right, FRET efficiency (E_A) for binned groups of cells plotted versus D_{free}[26,41] (CFP–CaM_{WT}), forming a binding isotherm[26,41]. Black symbols represent mean ± s.e.m. of four or five cells. To measure D_{free}, microscopic-specific units were calibrated to μM using the horizontal green scale bar[24], which represents 5 μM, here and in **e**–**g**. Half-maximal E_A was reached at $K_{d,EFF}$ = 700 D_{free} units, yielding $K_{a,EFF}$ = (1/$K_{d,EFF}$) = 143 × 10^{-5} (D_{free}^{-1} units), which is equivalent to K_a ~44 μM^{-1}. (**e**) FRET analysis for CaBP4–CFP versus $Ca_V1.3$–YFP. Black symbols represent mean ± s.e.m. of seven or eight cells. $K_{a,EFF}$ ~14 × 10^{-5} (D_{free}^{-1} units) or K_a ~4.4 μM^{-1}. (**f**) FRET 2-hybrid analysis for CaBP4–CFP versus YFP–IQ. Left, cartoon of FRET partners. Right, corresponding binding curve (black); symbols represent mean ± s.e.m. of five or six cells. Gray line represents the fit to holochannel relation from **e**. (**g**) FRET 2-hybrid analysis for CaBP4–CFP versus YFP–PCI peptide. Black symbols represent mean ± s.e.m. of seven or eight cells. (**h**) Cartoon of main α_{1D} subunit of $Ca_V1.3$, comprising four homologous domains, with intracellular loops (dark blue) facing downward. Red areas represent potential CaBP binding regions based on peptide FRET 2-hybrid analysis.

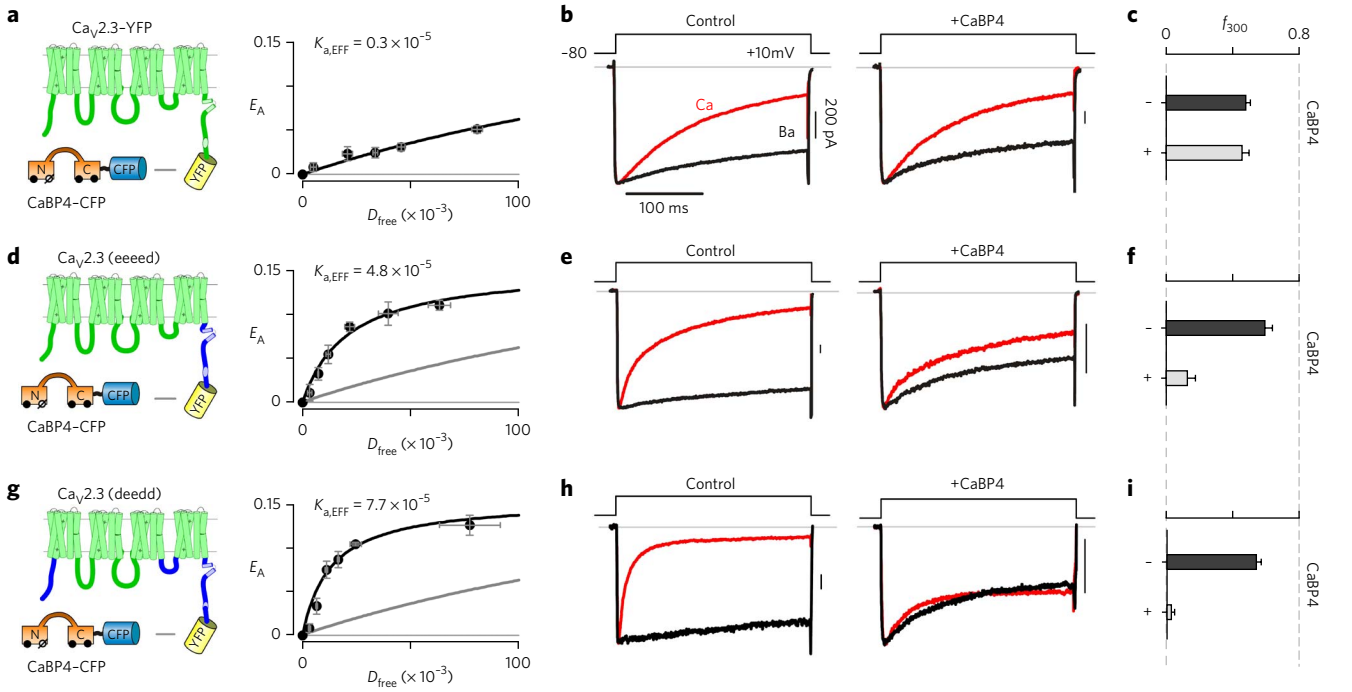

Figure 3 | Chimeric channels reveal the importance of CaBP sites beyond the IQ domain. (**a**–**c**) No CaBP4 binding or functional modulation of wild-type $Ca_V2.3$. (**a**) FRET experiment for $Ca_V2.3$ fused to YFP versus CaBP4-CFP, revealing little binding. Each symbol represents mean ± s.e.m. of approximately four or five cells. (**b**) Exemplar whole-cell current traces illustrating the absence of CaBP4's effect on CDI. (**c**) Population data confirm lack of CaBP4 effects on CDI. Bars average $n = 5$ cells each. (**d**) Left, cartoon of holochannel FRET experiment, pitting CaBP4-CFP versus YFP-tagged chimeric $Ca_V2.3$ with $Ca_V1.3$ CI substitution (eeeed). Right, increased binding affinity of eeeed with CaBP4 (each symbol represents mean ± s.e.m. of approximately three or four cells) compared to the control in gray (from **a**). (**e**) Exemplar whole-cell currents now exhibit partial CDI suppression by CaBP4. (**f**) Population data confirms partial CDI suppression by CaBP4 in eeeed channels. The control bar shows an average of $n = 5$ cells. The light gray bar for the CaBP4 condition shows an average of $n = 7$ cells. (**g**) Chimeric $Ca_V2.3$ channels that include the $Ca_V1.3$ amino terminus, III-IV loop and CI module (deedd) show the strongest CaBP4 binding (symbols show mean ± s.e.m. of approximately five cells each). (**h**) Exemplar whole-cell currents show complete CDI elimination by CaBP4. (**i**) The population average confirms the trend shown in **h**. The control bar graph shows an average of $n = 8$ cells, and the light gray bar for the CaBP4 condition shows an average of n cells.

Supplementary Fig. 3a), which readily forms functional chimeras with Ca_V1 channels[28,42]. FRET between CaBP4-CFP and $Ca_V2.3$ fused to YFP revealed little binding (**Fig. 3a**). Moreover, CaBP4 also did not influence CDI (**Fig. 3b**,**c**). Thus, $Ca_V2.3$ channels served as a 'blank slate', lacking both binding and modulation by CaBP4. First, we replaced the CI region of $Ca_V2.3$ with the corresponding segment of $Ca_V1.3$ (**Fig. 3d**). CaBP4 then bound appreciably to this chimeric channel (**Fig. 3d**). More importantly, CDI in these chimeric channels could now also be attenuated, though not eliminated, by CaBP4 (**Fig. 3e**,**f** and **Supplementary Fig. 3b**). Further chimeric-channel experiments indicated that adding both the amino terminus and III-IV loops of $Ca_V1.3$ were required for full CaBP4 sensitivity (**Supplementary Figs. 3** and **4**). The final outcome is demonstrated by the chimeric channel (**Fig. 3g**) containing all three candidate binding sites (amino terminus, III-IV loop and CI region) of $Ca_V1.3$. CaBP4 binding to this chimera shows the highest affinity (**Fig. 3g** and **Supplementary Fig. 3e**), and CDI is now completely eliminated by CaBP4 (**Fig. 3h**,**i** and **Supplementary Fig. 3d**). Direct deletions and mutagenesis performed on the $Ca_V1.3$ channel backbone further confirmed the functional contribution of all of these segments to CaBP4 sensitivity (**Supplementary Figs. 5**–**7**). Overall, the $Ca_V1.3$ CI region seemed necessary, and all three segments (amino terminus, III-IV, PCI and IQ) together were required for full functional sensitivity to CaBP4.

CaM and CaBP4 concurrently bind holochannels

With ample evidence for the functional contribution of CaBP binding beyond the IQ module, we pursued definitive tests for competitive versus allosteric interaction between CaM and CaBP4 (**Fig. 1b**). A crucial discriminator would be the presence or absence of simultaneous ligand binding and modulation of holochannels. Such a test would establish or exclude the existence of state 4 (**Fig. 1b**), thus furnishing a decisive mechanistic distinction.

To this end, we covalently fused CaM or CaBP4 to $Ca_V1.3$ channels, a strategy we used previously with functional assays alone to probe CaM interactions with $Ca_V1.2$ channels[43]. **Figure 4a**,**b** introduces the approach, here applied anew to $Ca_V1.3$ channels. To start, we considered $Ca_V1.3$ channels without covalently linked CaM, which again demonstrate robust CDI (**Fig. 4a**), just as observed earlier. Upon strong overexpression of a dominant-negative mutant CaM[9,14] (CaM_{1234}), which is Ca^{2+} insensitive, CDI is completely eliminated[14] (**Fig. 4a**). This outcome occurs because CaM_{1234} has competitively replaced endogenous functional CaM on the channel IQ domain[24]. By contrast, when the analogous experiment is performed with $Ca_V1.3$ channels fused to a single CaM (**Fig. 4b**), a completely different outcome results. Before coexpressing CaM_{1234} (**Fig. 4b**), these channels undergo robust CDI, indicating unfettered functionality of the covalently attached CaM. Notably, however, the covalent linkage of a single CaM would greatly enrich the local concentration of CaM to levels extending into the millimolar range[43]. This local concentration would far surpass the concentrations of CaM_{1234} achievable by expression as a separate molecule[24] (~10 μM). One would thereby predict that separately coexpressing CaM_{1234} in this context would have little or no effect on CDI. Indeed, we observed exactly this preservation of CDI (**Fig. 4b** and **Supplementary Fig. 8a**,**b**).

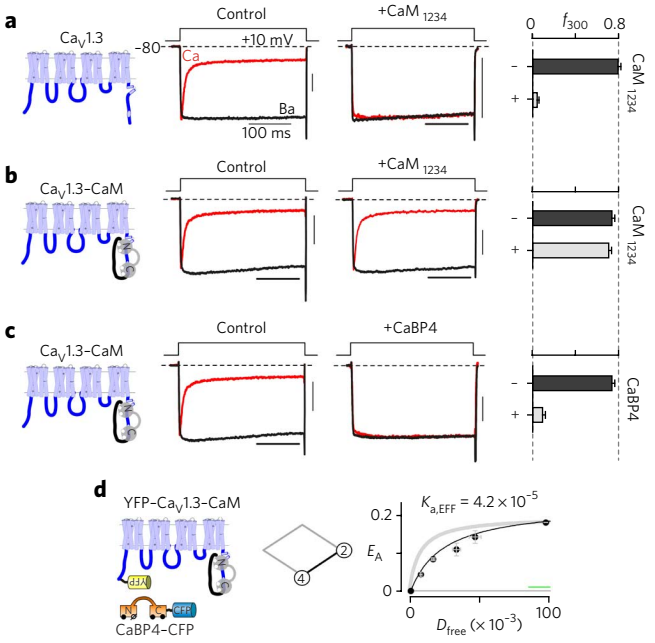

Figure 4 | CaBP4 and CaM simultaneously bind Ca$_V$1.3 channels. (**a**) The Ca^{2+}-insensitive mutant CaM (CaM_{1234}) completely eliminates CDI. Left, schematic of wild-type Ca$_V$1.3 channel. Control exemplar traces illustrate the baseline CDI for reference. +CaM_{1234} traces illustrate the complete loss of CDI upon CaM_{1234} coexpression. The bar graphs confirm the complete elimination of CDI by CaM_{1234} in population, where bars show an average of n = 5 cells each. (**b**) Complete occlusion of CaM_{1234} effects in Ca$_V$1.3 channels attached at the carboxy terminus to wild-type CaM via a 12-glycine linker (Ca$_V$1.3–CaM in left schematic). Control traces show robust CDI, indistinguishable from that in Ca$_V$1.3 channels lacking covalent linkage. By contrast, +CaM_{1234} exemplar traces illustrate complete sparing of CDI. Bar graph summaries confirm this trend, where each bar averages n = 6 cells each. (**c**) CaBP4 effects on Ca$_V$1.3–CaM. Control whole-cell current traces reproduced from **b** for reference. Remarkably, coexpressing CaBP4 with Ca$_V$1.3–CaM here completely eliminates CDI in both exemplar traces (+CaBP4) and in population bar graph data, where the dark control bar shows an average of n = 6 cells, and the light gray bar for the CaBP4 condition shows an average of n = 7 cells. (**d**) CaBP4 can still bind Ca$_V$1.3–CaM, where black symbols show mean ± s.e.m. of approximately five or six cells each. As a reference, the gray curve plots the amplitude-normalized fit obtained without CaM fusion from **Figure 3e**.

This outcome demonstrates that covalently attached CaM effectively occludes the IQ module in Ca$_V$1.3.

Thus armed, we could perform a pivotal experiment to test the effect of coexpressing CaBP4 with the Ca$_V$1.3–CaM construct. If CaBP4 and CaM compete at the IQ module, then CaBP4 should hardly influence CDI of Ca$_V$1.3–CaM, just as observed for CaM_{1234} (**Fig. 4b**). In contrast, we observed complete elimination of CDI (**Fig. 4c**), as confirmed by population data (**Fig. 4c** and **Supplementary Fig. 8c**). We also observed similar outcomes with CaBP1 acting on Ca$_V$1.3–CaM (**Supplementary Fig. 9**) as well as with CaBP modulation of analogous Ca$_V$1.2–CaM channels (**Supplementary Fig. 10**). These remarkable results strongly argue that CaBP and CaM can bind distinct sites on the channel, in contradiction to a competitive mechanism (**Fig. 1b**).

We advanced the approach of tethered CaM even further and directly corroborated the functional result above with holochannel binding assays involving Ca$_V$1.3–CaM. Holochannel FRET 2-hybrid analysis demonstrated that CaBP4 still binds Ca$_V$1.3–CaM (**Fig. 4d**), with only moderately reduced affinity compared to channels without covalently linked CaM (**Fig. 4d**). Markedly, owing to occlusion of the CaM binding site by tethered CaM, the binding of CaBP4 to Ca$_V$1.3–CaM directly probes transitions between states 2 and 4 (**Fig. 4d**). This yields an association constant K_{24} = 1.3 ± 0.2 μM^{-1}. Thus, we would argue that state 4 in **Figure 1b** exists.

A key remaining issue was the possibility of more than one CaBP4 molecule working together to modulate channels. Accordingly, we extended our linkage strategy still further and fused a single CaBP4 to the amino terminus of a channel that already had a carboxy-tail linkage to CaM. This created the dual-linkage construct in **Figure 5a**. Remarkably, this single CaBP4 entirely eliminated CDI, demonstrating that only one CaBP4 molecule suffices for full modulation (**Fig. 5a** and **Supplementary Fig. 8d**). Furthermore, FRET 2-hybrid assays between CaBP4–Ca$_V$1.3–YFP holochannels and CaBP4–CFP resulted in negligible binding (**Fig. 5b**), demonstrating explicitly that only a single CaBP4 can bind the channel. In this dual-linkage construct, the fused CaBP4 must certainly be interacting with the channel, otherwise CDI would not have been eliminated. Yet, the tethered CaM might conceivably be dislodged, retaining affiliation only via its linker. This possibility was excluded, however, because holochannel FRET assays confirmed that CaM, as a separate molecule, can indeed bind holochannels fused to CaBP4 (**Fig. 5c**). Because of occlusion of the CaBP4-binding pocket by linked CaBP4, binding of CaM to CaBP4–Ca$_V$1.3 directly probes transitions between states 3 and 4 (**Fig. 5c**), with an association constant K_{34} = 10 ± 2 μM^{-1}. Moreover, the maximal FRET efficiency at large D_{free} values ($E_{A/max}$) is indistinguishable from that for the corresponding experiment with Ca$_V$1.3 channels without fusion (**Fig. 3d**). Thus, apoCaM seems to bind holochannels in largely the same configuration, whether CaBP is present or not.

In all, these results argue that CaBP4 and CaM can bind concurrently to Ca$_V$1.3 channels. Although apoCaM most likely interacts with the IQ domain[24], CaBP4 modulation may rely on binding to elements outside the IQ domain.

Modulation by trace CaBP levels explained

That shown, how could trace concentrations of CaBPs modulate channels in excess CaM (**Fig. 1c–h**)? Accordingly, we elaborated on the four-state scheme of **Figure 1b** by including relevant association constants obtained above (**Figs. 2d**,**e**; **4d**; and **5c**). **Figure 6a** displays the result, which comprises a thermodynamic cycle of CaM and CaBP interaction with channels. Thus viewed, it was reassuring that $(K_{12} \times K_{24})/(K_{13} \times K_{34}) \approx 1$, in accord with thermodynamic constraints[44]. We thus proceeded to in-depth analysis of this scheme. If CaBP4 were to interact in a purely competitive manner, state 4 would not exist. Given a rough estimate of free endogenous CaM at 10 μM[25], the remaining three-state system would predict that a CaBP concentration of 107 μM would be required for half block of CDI (**Fig. 6b**). This concentration of CaBP4 far exceeds that generally present in the brain (**Fig. 1c–h**). If state 4 is included, so that an allosteric mechanism pertains, a very different outcome arises. In particular, if the binding of CaM and CaBP4 were completely independent, then transitions into state 4 would be governed by association constants K_{34} and K_{24}, which would be identical to K_{12} and K_{13}, respectively. Alternatively, if the transitions were to interact cooperatively, then K_{34} and K_{24} would be equal to K_{12} and K_{23} multiplied by a common factor λ that derives from thermodynamic mandates[44]. Here, λ > 1 would signify positive cooperativity in the binding of CaBP4 and CaM to the channel, λ < 1 would denote negative cooperativity, and λ = 0 would correspond to purely competitive binding of CaM and CaBP4. Markedly, our experiments permitted direct determination of the λ factor. K_{34} is lower than K_{12} by about fourfold, as is K_{24} compared to K_{13}. Thus, we estimate λ to be ~0.23, confirming a modest degree of negative cooperativity in the binding of

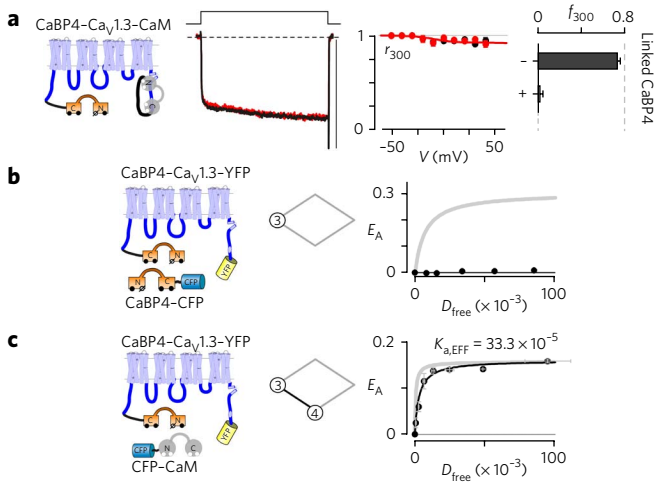

Figure 5 | Only one CaBP4 can bind per $Ca_V1.3$ channel. (**a**) The fusion of both CaBP4 (by 8-glycine linker) and CaM (by 12-glycine linker) to $Ca_V1.3$ ($CaBP4\text{-}Ca_V1.3\text{-}CaM$, cartoon at left) completely eliminates CDI, as seen from exemplar traces (middle left), overlay of Ba^{2+} (black) and Ca^{2+} (red) r_{300} relations (middle right, $n = 5$ cells per condition) and bar graph f_{300} (each bar shows an average of $n = 5$ cells). (**b**) CaBP4-CFP does not bind $CaBP4\text{-}Ca_V1.3\text{-}YFP$ (left schematic showing $Ca_V1.3$ channel with CaBP4 fused to its N terminus and YFP to its C terminus), suggesting that only one CaBP4 can bind $Ca_V1.3$. Middle diamond schematic indicates that $CaBP4\text{-}Ca_V1.3\text{-}YFP$ cannot be perturbed from state 3 by overexpressing CaBP4-CFP as a separate molecule. Black symbols each represent mean ± s.e.m. of three or four cells. The reference gray fit represents CaM binding to $Ca_V1.3$ channels lacking a fused CaBP4 (**Fig. 3e**). (**c**) Holochannel FRET indicates that CaM can still bind $CaBP4\text{-}Ca_V1.3\text{-}YFP$. Right, corresponding CFP-CaM binding curve (black symbols represent mean ± s.e.m. of approximately three or four cells each). The amplitude-normalized reference gray fit represents CaM binding $Ca_V1.3$ channels not fused to CaBP4 (**Fig. 3e**).

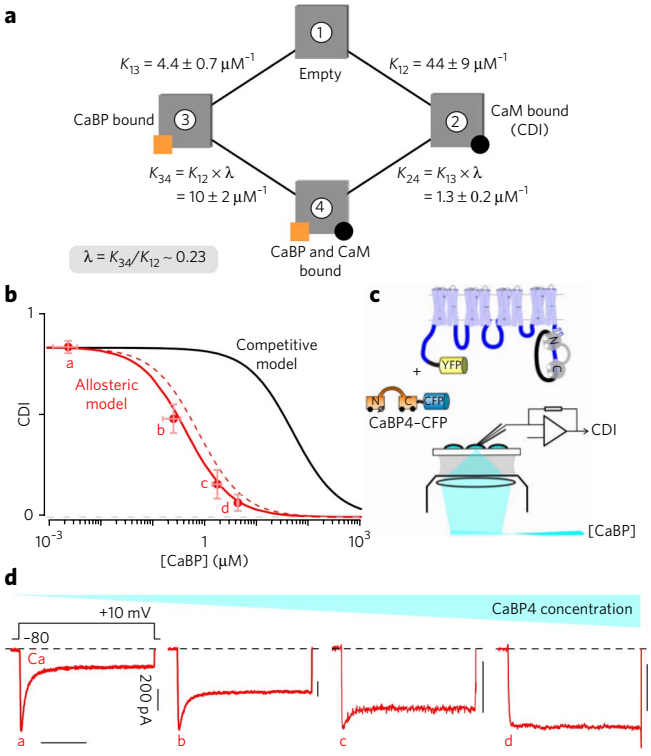

Figure 6 | Mechanism of $Ca_V1.3$ channel modulation by modest levels of CaBP4. (**a**) Allosteric model of CaM and CaBP4 binding to $Ca_V1.3$ channels (based on **Fig. 1b**) but now with experimentally determined association constants as listed and drawn from **Figures 2d,e**; **4d** and **5c**. (**b**) Model predictions for CaBP4 dependence of CDI. The relation that results under estimated free CaM of 10 μM if dual-bound state 4 does not exist (i.e., pure competition) is represented by the solid black line. The entire 4-state allosteric scheme, with experimentally determined association constants, predicts the red dashed curve for CDI dependence upon free CaBP concentration. The solid red curve fits experimental data from the approach outlined in **c**, where symbols each represent mean ± s.e.m. of $n = 5$ cells. (**c**) Schematic of patch fluorometry experiments. (**d**) Top, schematic for increasing CaBP4 concentration. Bottom, Ca^{2+} traces corresponding to various symbols in **b**, as labeled. Scale bar, 100 ms.

both CaBP4 and apoCaM to channels. Notably, given this precise diamond-shaped system, the projected effects of CaBP4 on CDI correspond to the red-dashed curve in **Figure 6b**, with a half CDI block at a CaBP4 concentration of ~0.8 μM. This concentration is plausibly consistent with levels in the brain. Moreover, accounting for the effects of endogenous CaM on our binding analysis produced little change in this prediction (**Supplementary Fig. 11** and **Supplementary Notes 1** and **2**). Thus, physiological CaBP4 may be able to exert modulation as a direct consequence of the allosteric mechanism in **Figure 6a**.

This notable prediction nonetheless relies on the accuracy of holochannel FRET assays. We thus used patch fluorometry to directly determine the sensitivity of $Ca_V1.3$ CDI to CaBP4 (**Fig. 6c**). Specifically, whole-cell electrophysiology measured CDI, and concurrent whole-cell fluorescence measurements estimated the concentration of fluorescently labeled CaBP4 molecules. CaM was fused to $Ca_V1.3$ channels to ensure a stable and high local concentration of CaM. Data thus obtained should decorate the predicted dashed-red curve in **Figure 6b**. Exemplar calcium traces (**Fig. 6d**) obtained under various CaBP4 concentrations illustrate variable CDI attenuation. Absent CaBP4 (**Fig. 6b,d**), the full measure of wild-type CDI is apparent. Notably, at estimated CaBP concentrations of less than 2.5 μM, CDI already exhibits substantial attenuation (**Fig. 6b,d**). Indeed, CDI becomes virtually absent at CaBP4 concentrations of 4 μM and higher (**Fig. 6b,d**). Population data corroborate these trends (**Fig. 6b**) and essentially overlay the predicted outcome from holochannel FRET assays (**Fig. 6b**). This correspondence substantiates our allosteric model (**Fig. 6a**) and its explanation for how trace amounts of CaBPs may exert their action on channels despite an abundance of CaM. As these experiments employed $Ca_V1.3$ fused covalently to CaM, the CaBP sensitivity here is a lower-limit estimate, making the outcome still more compelling.

DISCUSSION

CaBPs tune the Ca^{2+} responsiveness of numerous Ca^{2+} signaling molecules regulated by CaM, thereby projecting influence over diverse biological processes[13,18,19,21]. Channel peptide studies and the homology between CaBPs and CaM support the view that CaBPs act by competitively replacing CaM on target molecules[14,22,27]. However, CaM expression far exceeds CaBP expression in the brain, raising questions about the ability of CaBPs to exert appreciable effects. To overcome the interpretive limitations of peptide studies, we devised functional and live-cell FRET interaction assays on $Ca_V1.3$ holochannels covalently linked to CaM, CaBP4 or both. Notably, $Ca_V1.3$ channels fused to CaM are still strongly modulated by CaBP4, and holochannel FRET assays directly confirm CaBP4 binding to such channels. These results firmly establish that apoCaM and CaBP4 can bind simultaneously, implicating an allosteric scheme that predicts and explains how trace CaBP4 can modulate channels in excess CaM. We directly confirm this prediction using patch fluorometry.

These results project a new view of CaBP modulation of $Ca_V1.3$ channels that incorporates our recent molecular model of CDI[24] (**Supplementary Fig. 12**). The channel–apoCaM complex in **Supplementary Figure 12a** corresponds to configuration 2 in **Figure 6a**. The C-terminal lobe of apoCaM interacts strongly with the IQ domain, and the N lobe engages more weakly with EF-hand regions. CDI occurs upon Ca^{2+}-CaM switching interactions to its effector sites (**Supplementary Fig. 12b**), with the N-lobe of Ca^{2+}-CaM embracing an N-terminal spatial Ca^{2+}-transforming element (NSCaTE) module in the channel N terminus and the C-lobe forming a tripartite complex with the channel IQ module and upstream EF-hand region. To overlay CaBP4, we positioned CaBP4 with major contacts on the N terminus, III-IV loop and EF-hand regions (**Supplementary Fig. 12c**, corresponding to **Fig. 6a**). During rest, CaBP and apoCaM may bind simultaneously because principal interaction sites seem distinct for the two ligands. This proposed arrangement retains strong interaction of the IQ domain with the C-lobe of apoCaM, based on interpreting the equivalent $E_{A/max}$ values in **Figures 2d** and **5c** as evidence that apoCaM adopts a similar bound configuration, whether CaBP is absent or also bound. As this equivalence could conceivably accommodate different apoCaM arrangements, the suggested configuration is provisional. That said, the proposed layout (**Supplementary Fig. 12c**) does project a potential steric clash between the N-lobe of apoCaM and CaBP4 at the EF-hand region, which nicely rationalizes the modest negative cooperativity factor of $\lambda \sim 0.23$. On Ca^{2+} elevation, access of Ca^{2+}-CaM to its effector sites may be inhibited by CaBP4 preoccupying nearby or partially overlapping sites, thus prohibiting CDI. In this regard, the mechanism of CDI inhibition may be a nuanced combination of allosteric and competitive mechanisms. Under resting Ca^{2+}, CaBP and apoCaM posture for baseline position via an allosteric mechanism (**Fig. 6a**); however, upon Ca^{2+} elevation, CDI fails to occur because CaBP occludes Ca^{2+}-CaM effector sites via a potentially competitive regime. This class of mechanism may generalize to other CaBP target molecules that share distinctions between sites for apoCaM preassociation and Ca^{2+}-CaM effectuation. $Ca_V1.2$ channels are homologous to $Ca_V1.3$ (ref. 45) and are likely to subscribe to an analogous mechanism. Ryanodine receptors are CaM regulated and exhibit movement of CaM between distinct apoCaM and Ca^{2+}-CaM sites[46]. Closely related IP3 receptors host binding sites for both apoCaM[47] and Ca^{2+}-CaM[48,49] and are modulated by CaBP[18,19].

More broadly, measuring binding and function in holomolecules fused to modulatory ligands may apply to many systems. Particular advantages include the ability to readily isolate individual transitions within cyclical binding schemes and the interpretive relevance of results obtained on holomolecules in live cells. Indeed, the approaches developed here enrich a burgeoning toolkit for pursuing quantitative biochemistry in functional assemblies within live cells. This endeavor promises rapid progress in understanding native molecular mechanisms[50].

Received 31 July 2013; accepted 25 November 2013; published online 19 January 2014

METHODS

Methods and any associated references are available in the online version of the paper.

References

1. Wang, L., Martin, B., Brenneman, R., Luttrell, L.M. & Maudsley, S. Allosteric modulators of G protein–coupled receptors: future therapeutics for complex physiological disorders. *J. Pharmacol. Exp. Ther.* **331**, 340–348 (2009).
2. Ritter, S.L. & Hall, R.A. Fine-tuning of GPCR activity by receptor-interacting proteins. *Nat. Rev. Mol. Cell Biol.* **10**, 819–830 (2009).
3. Li, Y., Krupa, B., Kang, J.S., Bolshakov, V.Y. & Liu, G. Glycine site of NMDA receptor serves as a spatiotemporal detector of synaptic activity patterns. *J. Neurophysiol.* **102**, 578–589 (2009).
4. Hynes, R.O. Integrins: bidirectional, allosteric signaling machines. *Cell* **110**, 673–687 (2002).
5. Alberts, B. *et al. Molecular Biology of the Cell* 3rd edn., 195–222 (Garland, 1996).
6. Goodey, N.M. & Benkovic, S.J. Allosteric regulation and catalysis emerge via a common route. *Nat. Chem. Biol.* **4**, 474–482 (2008).
7. Grunwald, M.E., Zhong, H., Lai, J. & Yau, K.W. Molecular determinants of the modulation of cyclic nucleotide-activated channels by calmodulin. *Proc. Natl. Acad. Sci. USA* **96**, 13444–13449 (1999).
8. Dunlap, K. Calcium channels are models of self-control. *J. Gen. Physiol.* **129**, 379–383 (2007).
9. Peterson, B.Z., DeMaria, C.D., Adelman, J.P. & Yue, D.T. Calmodulin is the Ca^{2+} sensor for Ca^{2+}-dependent inactivation of L-type calcium channels. *Neuron* **22**, 549–558 (1999).
10. Zühlke, R.D., Pitt, G.S., Deisseroth, K., Tsien, R.W. & Reuter, H. Calmodulin supports both inactivation and facilitation of L-type calcium channels. *Nature* **399**, 159–162 (1999).
11. Alseikhan, B.A., DeMaria, C.D., Colecraft, H.M. & Yue, D.T. Engineered calmodulins reveal the unexpected eminence of Ca^{2+} channel inactivation in controlling heart excitation. *Proc. Natl. Acad. Sci. USA* **99**, 17185–17190 (2002).
12. Haeseleer, F. *et al.* Five members of a novel Ca^{2+}-binding protein (CABP) subfamily with similarity to calmodulin. *J. Biol. Chem.* **275**, 1247–1260 (2000).
13. Haeseleer, F. *et al.* Essential role of Ca^{2+}-binding protein 4, a Cav1.4 channel regulator, in photoreceptor synaptic function. *Nat. Neurosci.* **7**, 1079–1087 (2004).
14. Yang, P.S. *et al.* Switching of Ca^{2+}-dependent inactivation of $Ca_V1.3$ channels by calcium binding proteins of auditory hair cells. *J. Neurosci.* **26**, 10677–10689 (2006).
15. Cui, G. *et al.* Ca^{2+}-binding proteins tune Ca^{2+}-feedback to Cav1.3 channels in mouse auditory hair cells. *J. Physiol. (Lond.)* **585**, 791–803 (2007).
16. Lee, S., Briklin, O., Hiel, H. & Fuchs, P. Calcium-dependent inactivation of calcium channels in cochlear hair cells of the chicken. *J. Physiol. (Lond.)* **583**, 909–922 (2007).
17. Lee, A. *et al.* Differential modulation of $Ca_V2.1$ channels by calmodulin and Ca^{2+}-binding protein 1. *Nat. Neurosci.* **5**, 210–217 (2002).
18. Yang, J. *et al.* Identification of a family of calcium sensors as protein ligands of inositol trisphosphate receptor Ca^{2+} release channels. *Proc. Natl. Acad. Sci. USA* **99**, 7711–7716 (2002).
19. Kasri, N.N. *et al.* Regulation of InsP3 receptor activity by neuronal Ca^{2+}-binding proteins. *EMBO J.* **23**, 312–321 (2004).
20. Zhou, H. *et al.* Ca^{2+}-binding protein-1 facilitates and forms a postsynaptic complex with Cav1.2 (L-type) Ca^{2+} channels. *J. Neurosci.* **24**, 4698–4708 (2004).
21. Haeseleer, F. & Palczewski, K. Calmodulin and Ca^{2+}-binding proteins (CaBPs): variations on a theme. *Adv. Exp. Med. Biol.* **514**, 303–317 (2002).
22. Oz, S. *et al.* Competitive and non-competitive regulation of calcium-dependent inactivation in $Ca_V1.2$ L-type Ca^{2+} channels by calmodulin and Ca^{2+}-binding protein 1. *J. Biol. Chem.* **288**, 12680–12691 (2013).
23. Findeisen, F. & Minor, D.L. Jr. Structural basis for the differential effects of CaBP1 and calmodulin on $Ca_V1.2$ calcium-dependent inactivation. *Structure* **18**, 1617–1631 (2010).
24. Ben Johny, M., Yang, P.S., Bazzazi, H.X. & Yue, D.T. Dynamic switching of calmodulin interactions underlies Ca^{2+} regulation of $Ca_V1.3$ channels. *Nat. Commun.* **4**, 1717 (2013).
25. Liu, X., Yang, P.S., Yang, W. & Yue, D.T. Enzyme-inhibitor-like tuning of Ca^{2+} channel connectivity with calmodulin. *Nature* **463**, 968–972 (2010).
26. Erickson, M.G., Liang, H., Mori, M.X. & Yue, D.T. FRET two-hybrid mapping reveals function and location of L-type Ca^{2+} channel CaM preassociation. *Neuron* **39**, 97–107 (2003).
27. Findeisen, F., Rumpf, C. & Minor, D.L. Apo states of calmodulin and CaBP1 control Ca_V1 voltage-gated calcium channel function through direct competition for the IQ domain. *J. Mol. Biol.* **425**, 3217–3234 (2013).
28. de Leon, M. *et al.* Essential Ca^{2+}-binding motif for Ca^{2+}-sensitive inactivation of L-type Ca^{2+} channels. *Science* **270**, 1502–1506 (1995).
29. Kim, J., Ghosh, S., Nunziato, D.A. & Pitt, G.S. Identification of the components controlling inactivation of voltage-gated Ca^{2+} channels. *Neuron* **41**, 745–754 (2004).
30. Dick, I.E. *et al.* A modular switch for spatial Ca^{2+} selectivity in the calmodulin regulation of Ca_V channels. *Nature* **451**, 830–834 (2008).
31. Oz, S., Tsemakhovich, V., Christel, C.J., Lee, A. & Dascal, N. CaBP1 regulates voltage-dependent inactivation and activation of $Ca_V1.2$ (L-type) calcium channels. *J. Biol. Chem.* **286**, 13945–13953 (2011).

32. Zhou, H., Yu, K., McCoy, K.L. & Lee, A. Molecular mechanism for divergent regulation of Cav1.2 Ca^{2+} channels by calmodulin and Ca^{2+}-binding protein-1. *J. Biol. Chem.* **280**, 29612–29619 (2005).
33. Lorenzen, A. & Schwabe, V. in *Purinergic and Pyrimidinergic Signalling I* (eds. Abbracchio, M.P. & Williams, M.) 19–34 (Springer-Verlag, 2001).
34. Logothetis, D.E., Lupyan, D. & Rosenhouse-Dantsker, A. Diverse Kir modulators act in close proximity to residues implicated in phosphoinositide binding. *J. Physiol. (Lond.)* **582**, 953–965 (2007).
35. Lein, E.S. *et al.* Genome-wide atlas of gene expression in the adult mouse brain. *Nature* **445**, 168–176 (2007).
36. Belgard, T.G. *et al.* A transcriptomic atlas of mouse neocortical layers. *Neuron* **71**, 605–616 (2011).
37. Blackshaw, S. *et al.* Genomic analysis of mouse retinal development. *PLoS Biol.* **2**, E247 (2004).
38. Colantuoni, C. *et al.* Temporal dynamics and genetic control of transcription in the human prefrontal cortex. *Nature* **478**, 519–523 (2011).
39. Vogel, C. & Marcotte, E.M. Insights into the regulation of protein abundance from proteomic and transcriptomic analyses. *Nat. Rev. Genet.* **13**, 227–232. 10.1038/nrg3185 (2012).
40. Chao, S.H., Suzuki, Y., Zysk, J.R. & Cheung, W.Y. Activation of calmodulin by various metal cations as a function of ionic radius. *Mol. Pharmacol.* **26**, 75–82 (1984).
41. Erickson, M.G., Alseikhan, B.A., Peterson, B.Z. & Yue, D.T. Preassociation of calmodulin with voltage-gated Ca^{2+} channels revealed by FRET in single living cells. *Neuron* **31**, 973–985 (2001).
42. Mori, M.X., Vander Kooi, C.W., Leahy, D.J. & Yue, D.T. Crystal structure of the Ca_V2 IQ domain in complex with Ca^{2+}/calmodulin: high-resolution mechanistic implications for channel regulation by Ca^{2+}. *Structure* **16**, 607–620 (2008).
43. Mori, M.X., Erickson, M.G. & Yue, D.T. Functional stoichiometry and local enrichment of calmodulin interacting with Ca^{2+} channels. *Science* **304**, 432–435 (2004).
44. Hill, T.L. *Free Energy Transduction in Biology: The Steady-State Kinetic and Thermodynamic Formalism* 64 (Academic Press, 1977).
45. Xu, W. & Lipscombe, D. Neuronal $Ca_V1.3\alpha1$ L-type channels activate at relatively hyperpolarized membrane potentials and are incompletely inhibited by dihydropyridines. *J. Neurosci.* **21**, 5944–5951 (2001).
46. Samsó, M. & Wagenknecht, T. Apocalmodulin and Ca^{2+}-calmodulin bind to neighboring locations on the ryanodine receptor. *J. Biol. Chem.* **277**, 1349–1353 (2002).
47. Bosanac, I. *et al.* Crystal structure of the ligand binding suppressor domain of type 1 inositol 1,4,5-trisphosphate receptor. *Mol. Cell* **17**, 193–203 (2005).
48. Lin, C., Widjaja, J. & Joseph, S.K. The interaction of calmodulin with alternatively spliced isoforms of the type-I inositol trisphosphate receptor. *J. Biol. Chem.* **275**, 2305–2311 (2000).
49. Yamada, M. *et al.* The calmodulin-binding domain in the mouse type 1 inositol 1,4,5-trisphosphate receptor. *Biochem. J.* **308**, 83–88 (1995).
50. Gough, N.R. Biochemistry: quantifying interactions. *Sci. Signal.* **3**, ec62 (2010).

Acknowledgments

We thank W. Yang for dedicated technical support and other members of the Ca^{2+} signals lab for valuable comments. H. Bazzazi generously made available the β_{2a}–CaM_{WT} construct. Y. Gao contributed the data analysis showing CaM, CaBP4 and CaBP1 gene expression from human prefrontal cortex. This work is supported by grants from the US National Institutes of Health (NIH) Heart, Lung, and Blood Institute MERIT Award (to D.T.Y.), NIH National Institute on Deafness and Other Communication Disorders (P.S.Y. and P. Fuchs), NIH National Institute of General Medical Sciences (GM08752 to P.S.Y.) and the NIH National Institute of Mental Health (M.B.J.).

Author contributions

P.S.Y. created mutant, chimeric and engineered channels. P.S.Y. and M.B.J. performed electrophysiology and FRET experiments and undertook extensive data analysis. M.B.J. performed molecular modeling. D.T.Y. supervised and helped conceive the project. All of the authors refined hypotheses, wrote the paper and created figures.

Competing financial interests

The authors declare no competing financial interests.

Additional information

Supplementary information is available in the online version of the paper. Reprints and permissions information is available online at http://www.nature.com/reprints/index.html. Correspondence and requests for materials should be addressed to D.T.Y.

ONLINE METHODS

Deep sequencing (RNA-seq) analysis of human prefrontal cortex. Extensive methods appear in a prior publication[38], available at GEO (GSE30272). Briefly, total mRNA was isolated to create a complementary DNA (cDNA) library for HiSeq2000 sequencing (Illumina). Pair-end reads of cDNA sequences were aligned to a human reference genome from UCSC Genome Bioinformatics and analyzed through custom software[51] (Maximum Oligonucleotide Mapping). Once all transcript reads have been mapped to various genes, the total number of reads mapping to a specific gene X is assigned the variable M_X. The length of that gene is given by L_X, and the total number of mapped reads is specified by R (in other words, $R = \Sigma M_X$, summed over all X). Accordingly, we can calculate the relative number of transcripts (RPKM) for each gene X, defined as $RPKM_X = (10^9 \times M_X)/(L_X \times R)$. In this manner, RPKM normalizes the number of reads to both the length of the gene and the extent of coverage across the entire deep-sequencing experiment. Thus, $RPKM_X$ enables direct comparison of relative transcript expression among different genes. Analogous methods were used for display of mouse deep sequencing analysis.

Normalization of *in situ* hybridization images. *In situ* hybridization images for CaM, CaBP1 and CaBP4, taken from spatially corresponding sagittal brain sections, were selected from the Allen mouse brain atlas (2012 Allen Institute for Brain Science; SectionData Set.id = 101343070 (CaM), 74453309 (CaBP1) and 70217701 (CaBP4); http://mouse.brain-map.org/). These images were normalized according to the relative transcript levels of CaBPs ($RPKM_{CaBP}$) and CaM ($RPKM_{CaM}$) in the mouse neocortex, as estimated from the deep sequencing analysis described above. Specifically, mean intensities ($\langle I_{CaM} \rangle$ and $\langle I_{CaBP} \rangle$) were computed as the average pixel value over the neocortical region. CaBP1 and CaBP4 images were then scaled by $SF = (RPKM_{CaBP} / RPKM_{CaM}) \times (\langle I_{CaM} \rangle / \langle I_{CaBP} \rangle)$ to make visible all expression profiles. All images (CaM, CaBP1, CaBP4) were then scaled uniformly before optimal display in **Figure 1**.

Molecular biology. All engineering of $Ca_V1.3$ (α_{1D}) was performed with rat α_{1D} (ref. 45) and $Ca_V2.3$ engineering with rat α_{1E} (ref. 42). Holochannel FRET constructs (**Figs. 2** and **3**) were constructed by fusing YFP shortly after the IQ domain in $Ca_V1.3$ (at amino acid 1626) and $Ca_V2.3$ (residue 1841). The details for the $Ca_V2.3$ fusions have been described[41]. For the $Ca_V1.3$ fusion, we first substituted a KpnI for the stop codon in α_{1D}. Then, a PCR product (encoding KpnI followed by eight glycines, YFP (with stop codon) and PmeI) was ligated into the KpnI site of α_{1D}, yielding the $Ca_V1.3$–YFP construct in **Figure 2d**. For FRET 2-hybrid peptide constructs (**Fig. 2f**,**g**), we replaced CaM of YFP–CaM[41] with appropriate PCR-amplified segments, via unique NotI and XbaI sites flanking CaM (**Supplementary Fig. 2**). CaBP1 and CaBP4 FRET constructs were described previously[14]. Chimeric $Ca_V2.3$ and $Ca_V1.3$ channels (**Fig. 3**) were constructed with overlap-extension PCR performed on α_{1D} and α_{1E} templates. Primers were designed to insert $Ca_V1.3$ segments (N-terminus residues 1–117, III-IV loop residues 1165–1216 and C-terminus residues 1467–1626) into corresponding regions of $Ca_V2.3$ channels, using appropriate unique restriction enzymes in $Ca_V2.3$. Specifically, PCR-based overlap extension using an α_{1D} template was used to create an N-terminal product incorporating a $\Delta NT_{83–108}$ deletion. This fragment was cloned into unique NheI (upstream of start) and BsiWI (within domain I) sites of α_{1D}, yielding the Δ83–108 construct in **Supplementary Figure 6**. Overlap extension was also used to substitute alanines within the III-IV loop region (34Lmut in **Supplementary Fig. 6**), with corresponding PCR product ligated into α_{1D} at unique ApaI and HindIII sites. Deletion of ΔpreIQ segment (**Supplementary Fig. 7**) was accomplished by first deleting the whole CI region in α_{1D} and replacing it with a PCR-amplified portion of the CI region (EF-hand region alone) that lacked a stop codon, via unique upstream BglII and downstream XbaI sites. Then, PCR product encoding an IQ domain preceded by a single glycine was ligated into unique upstream XbaI and downstream PmeI sites. To link CaM to constructs in **Figure 4**, we created a PCR product encoding upstream XbaI preceding 12 glycines, followed by CaM, a stop codon and SpeI. This product was ligated into corresponding α_{1D} constructs, which contained a unique XbaI just before Gly1626. Similarly for β_{2a}-CaM (**Supplementary Fig. 7**), we deleted the stop codon of rat β_{2a} and introduced an NotI site for inserting a XbaI-$glycine_8$-CaM-ApaI product. To attach YFP to the N terminus of $Ca_V1.3$–CaM (**Fig. 4d**), we substituted a unique NheI for the start segment. Then we created a PCR product encoding an upstream NheI, followed by YFP (stopless), six glycines and AvrII. This product was ligated into the unique NheI site of $Ca_V1.3$–CaM. Similarly, to link a single CaBP4 (**Fig. 5a**), an analogous PCR-amplified CaBP4 product was cloned in an identical fashion. To create the channel construct in **Figure 5b**, the NheI-BsiWI fragment of the construct in **Figure 5a** (includes CaBP4 fusion to channel N terminus) was swapped into the corresponding sites of $Ca_V1.3$–YFP (**Fig. 2d**). All of the segments subject to PCR were verified by sequencing.

Transfection of HEK293 cells. For electrophysiology, HEK293 cells were cultured on 10-cm plates and transiently transfected by a calcium-phosphate protocol. We combined 8 μg each of cDNAs encoding channel α_1 subunit, rat brain β_{2a} (M80545) and rat brain $\alpha_{2\delta}$ (NM012919.2) and 1–2 μg of SV40 T antigen. For experiments with mouse CaBP4 and human CaBP1, 8 μg of inducible expression plasmid (pIND) vector (Invitrogen, San Diego, CA) encoding CaBP fused with GFP (CaBP-GFP) was also cotransfected; after recombinant channels exhibited robust currents, CaBPs were expressed 8–10 h on induction by 1 μM muristerone A (insect hormone analog). Holochannel FRET 2-hybrid experiments were transfected with PEI according to manufacturer protocols (Polysciences, Warrington, PA). All of the subunits were driven by a CMV promoter. Experiments were generally performed 1–3 d after transfection.

FRET 2-hybrid assay. FRET 2-hybrid assays were performed as described[26] in HEK293 cells and carried out in 2 mM Ca^{2+} Tyrode's buffer. All of the assays were performed under resting intracellular Ca^{2+} conditions, where apoCaM predominates[26,41]. In rare instances where plateaus of FRET binding curves were not explicitly constrained by data, we assumed a maximal E_A value of 0.116, so as to permit a nominal estimate of $K_{a,EFF}$. The placement of fluorescent tags on CaM and CaBP was chosen to preserve functional interaction with channels, as assessed by electrophysiology. For simultaneous CaBP4-CFP concentration imaging and patch-clamp recording, CFP fluorescence intensity measurements were obtained before whole-cell break-in and did not change appreciably thereafter. These experiments used the standard electrophysiological recording bath solutions described below. CaBP concentrations were estimated from whole-cell CFP fluorescence intensity S_{CFP} as follows[24,26]: $[CaBP] = (S_{CFP}/M_D) \times 0.0000326\ (\mu M/D_{free})$, where M_D was estimated to be 0.0992137 (ref. 26).

Whole-cell electrophysiology. Whole-cell recordings were obtained at room temperature in transfected HEK293 cells (Axopatch 200A, Axon Instruments). Electrodes were pulled from borosilicate glass capillaries (World Precision Instruments, MTW 150-F4), with 1–3 MΩ resistances, before 80% series resistance compensation. Currents were filtered at 2 kHz, and a P/8 leak-subtraction protocol was used. The internal solution contained for $Ca_V1.3$ and chimeric $Ca_V2.3$ channels: $CsMeSO_3$, 114 mM; $CsCl_2$, 5 mM; $MgCl_2$, 1 mM; MgATP, 4 mM; HEPES (pH 7.4), 10 mM; and BAPTA, 10 mM; at 295 mOsm adjusted with $CsMeSO_3$. The high sensitivity of CDI to local Ca^{2+} influx in these channels allowed convenient use of elevated intracellular Ca^{2+} buffering. The internal solution contained for $Ca_V2.3$ channels: $CsMeSO_3$, 135 mM; $CsCl_2$, 5 mM; $MgCl_2$, 1 mM; MgATP, 4 mM; HEPES (pH 7.4), 10 mM; and EGTA, 0.5 mM; at 295 mOsm adjusted with $CsMeSO_3$. CDI of these channels requires global elevation of Ca^{2+} in cells, necessitating the use of modest intracellular Ca^{2+} buffering. External solutions contained: TEA-$MeSO_3$, 102 mM; HEPES (pH 7.4), 10 mM; and $CaCl_2$ or $BaCl_2$, 40 mM; at 300 mOsm, adjusted with TEA-$MeSO_3$.

Biochemical modeling of CaBP inhibition of Ca_V1 CDI. We considered both mixed allosteric and strictly competitive inhibition models to assess the concentration dependence of CaBP action on Ca_V1 channels. For the allosteric model, we analyzed the model presented in **Figure 6a**. Here, only channels in configuration 2 are able to undergo normal CDI. Thus,

$$CDI = CDI_{max} \frac{K_{12} \cdot [CaM]}{1 + K_{12} \cdot [CaM] + K_{13} \cdot [CaBP] + K_{34} \cdot K_{13} \cdot [CaM] \cdot [CaBP]}$$

where CDI_{max} is the CDI strength that would be observed if all channels reside in configuration 2 at the beginning of an activating voltage pulse. The association constants K_{12}, K_{13}, K_{34} were estimated from FRET binding experiments as

summarized in **Figure 6a**. For simulations, the ambient [CaM] concentration was assumed to be 10 μM[25]. Importantly, thermodynamic constraints mandate that $K_{24} = K_{13} \cdot K_{34}/K_{12}$, a condition validated experimentally. In the strictly competitive model, we set $K_{34} = 0$, thus allowing channels to only populate configurations 1, 2 and 3.

Molecular modeling. Molecular models and atomic structures in **Supplementary Figure 12a**,**b** were previously described[24]. **Supplementary Figure 12c** was created by adjusting the configuration in **Supplementary Figure 12a**, through changes in backbone dihedral angles within the linker between apoCaM lobes, permitting the approximate dimensions of CaBP to engage the EF-hand region.

51. Eaves, H.L. & Gao, Y. MOM: maximum oligonucleotide mapping. *Bioinformatics* **25**, 969–970 (2009).

doi:10.1038/nchembio.1436